Exploring the catalytic properties of palladium supported catalysts in transfer hydrogenolysis of glycerol

F. Mauriello[1,*], H. Ariga[2], M.G. Musolino[1], R. Pietropaolo[1], S. Takakusagi[2], and K. Asakura[2,*]

[1] *Dipartimento di DICEAM, Università Mediterranea di Reggio Calabria, Loc. Feo di Vito, I-89122 Reggio Calabria, Italy*

[2] *Catalysis Research Center, Hokkaido University, Kita-ku N21W10, Sapporo, Hokkaido 001-0021, Japan*

**Corresponding authors.*

Tel: +39 0965875278 Fax: +39 0965875248
E-mail: francesco.mauriello@unirc.it. (F. Mauriello)

Tel and Fax: +11-706-9113
E-mail: askr@cat.hokudai.ac.jp. (K. Asakura)

Keywords: Catalytic Transfer hydrogenolysis (CTH), Glycerol valorization, 1,2-Propanediol, Coprecipitated palladium catalysts, Strong Metal Support Interaction.

Abstract

The transfer hydrogenolysis of glycerol promoted by palladium based catalysts is reported. The reactions were carried out under mild conditions (453 K and 5 bar of N_2) in absence of added hydrogen by using the reaction solvent, 2-propanol, as hydrogen source. The catalytic results were interpreted in terms of metal (Pd)-metal (Co or Fe) interaction that modifies the electronic properties of palladium and affords bimetallic PdM sites (M = Co or Fe), thus enhancing the catalytic properties of the systems in the conversion of glycerol as well as in the selectivity to 1,2-propanediol and 1-propanol. The transfer hydrogenolysis mechanism is here elucidated and involves the glycerol dehydration to 1-hydroxyacetone and the subsequent hydrogenation of 1-hydroxyacetone to propylene glycol.

1. Introduction

The use of renewable biomass for bulk chemicals production provides a viable route for the modern chemical industry to alleviate its historical dependence on fossil resources and to reduce, at the same time, CO_2 emissions [1]. Among several catalytic processes for upgrading biomass derived compounds, "bio"-hydrogenolysis has gained a lot of attention in recent years, bearing the potential to bridge available technologies and future refinery concepts [2]. Surely, one of the main targets is currently to make the hydrogenolysis a self-sustainable process and to reduce the costs related to hydrogen purchase, transport and storage and to minimize safety problems in industrial hydrogenation processes. Catalytic transfer hydrogenolysis (CTH) reactions [3] represent an interesting alternative to the direct use of molecular hydrogen. Together with traditional hydrogen donors (cyclohexane, hydrazine, formic acid and formiats), simple alcohols such as ethanol and 2-propanol can be used in CTH with primary alcohols generally less active than secondary alcohols due to the smaller electron-releasing inductive effect.

Glycerol is the major by-product in the industrial production of biodiesel and it is also a model molecule for biomass derived polyols keeping the potential to become a new primary building block [4]. Indeed, glycerol can be converted, through the hydrogenolysis reaction, into valuable products such as 1,2-propanediol (1,2-PDO), 1,3-propanediol (1,3-PDO) and ethylene glycol (EG), widely used in the synthesis of polyester fibers and resins, pharmaceuticals, cosmetics, flavours and fragrances, antifreeze, among others [5].

While several metal catalysts, including supported Cu, Ru, Rh, Pt and Ni, have been widely studied in the hydrogenolysis of glycerol, palladium has not been investigated significantly. In recent years co-precipitated palladium catalysts, and, in particular, coprecipitated palladium on iron oxide, have been deeply investigated showing superior performance in a number of reactions such as: CO oxidation [6], aqueous-phase reforming of ethylene glycol [7], aliphatic carbonyl reduction [8] and biomass derived polyols hydrogenolysis [9]. Furthermore it was reported that palladium, if properly supported, can be

chosen as catalytic active centre in glycerol CTH hydrogenolysis [10]: high conversion and selectivity to 1,2-PDO were easily obtained with catalysts prepared by the coprecipitation technique

It is generally accepted that catalysts, prepared by the coprecipitation technique, are characterized by an intimate interaction between the active metal and the oxide-support; furthermore mixture of single/mixed oxides phases and not uniform distribution of active metal do also occur [11]. This complexity, by itself, does not allow to fully understand the role of the different components in coprecipitated catalysts. In this context, a comparison between the catalytic activity of palladium catalysts supported on iron oxide and cobalt oxide prepared both by coprecipitation and impregnation techniques in the catalytic transfer hydrogenolysis of glycerol should be widely welcome.

The present study aims to clarify the effect of individual parameters such as surface area, metal particle size, oxidation state of palladium, role of the support and presence of bimetallic clusters that may affect the catalytic properties of palladium catalysts in transfer hydrogenolysis of glycerol. More fundamental understanding might, in fact, help a further and more rational optimization of the synthesis parameters in order to drive the catalytic properties of coprecipitated catalysts. Therefore, X-ray diffraction (XRD), transmission electron microscopy (TEM), temperature-programmed reduction by H_2 (H_2-TPR) and X-ray photoelectron spectroscopy (XPS) were performed to characterize structures and surface properties of palladium catalysts.

The catalytic conversion of glycerol to 1,2-PDO and EG was carried out in absence of additional H_2 with the solvent (2-propanol) being the source of the necessary hydrogen. Comparison of results involves, on one hand, coprecipitated PdCo and PdFe catalysts and, on the other hand, impregnated Pd/Co_3O_4, Pd/CoO, Pd/Fe_2O_3 and Pd/Fe_3O_4 samples as well as model catalysts such as commercial Pd/SiO_2. This broad set of Pd catalysts was chosen to get a wide framework of the factors that characterize the catalysts behaviour.

The relationship between the physico-chemical properties of palladium based catalysts and their catalytic performance is highlighted. The final aim is to put a deep insight on factors that make

palladium coprecipitated systems very peculiar and unique, among palladium containing catalysts, in affording glycerol hydrogenolysis. The correlation of the physicochemical properties of the investigated Pd-based catalysts with the CTH of glycerol suggests that the catalyst preparation plays a crucial role in determining the electronic properties of palladium through strong interaction with the metal oxide support so that unusual catalytic properties can be obtained.

Moreover, a thorough examination of the reaction mechanism is included with hydroxyacetone being the key-intermediate in the catalytic transfer hydrogenolysis reaction. Finally, an insight is also given to understand if the nature of the catalyst influences the dehydrogenation of the alcoholic solvent, the single steps of glycerol reduction or both processes occurring in the overall reaction.

2. Experimental Section

2.1 Catalysts preparation

All chemicals were purchased from Sigma-Aldrich and used without further purification.

Catalysts preparation: supported palladium catalysts were obtained by using two different techniques: coprecipitation and impregnation. PdCo and PdFe catalysts were prepared by using the coprecipitation technique, with a nominal palladium loading of 5 wt %, and were obtained from aqueous solutions of the corresponding inorganic precursors. Anhydrous palladium chloride (Fluka, purum, 60 % palladium) was dissolved in HCl and cobalt(II) nitrate hexahydrate (Fluka, purity ≥ 99 %) or iron(III) nitrate nonahydrate (Fluka, purity ≥ 98 %) were added. The obtained aqueous metal salt solutions were added dropwise into a 1 M aqueous solution of Na_2CO_3. After filtration, samples were washed until complete removal of chloride ions, dried for 1 day at 353 K and further reduced at 473 K for 2h under a flow of hydrogen.

Catalysts prepared by incipient wetness impregnation (Pd/Co_3O_4, Pd/CoO, Pd/Fe_3O_4 and Pd/Fe_2O_3) were obtained by adding a solution of palladium(II) acetylacetonate (Aldrich, purity 99 %) dissolved in acetone to commercially available supports Co_3O_4 (Aldrich, SBET=40-70 $m^2 g^{-1}$), CoO (Aldrich, SBET=7 $m^2 g^{-1}$), Fe_2O_3 (Sigma–Aldrich, SBET=4 $m^2 g^{-1}$) and Fe_3O_4 (Aldrich, SBET=60 $m^2 g^{-1}$). After impregnation, samples were dried for 1 day under vacuum at 353K and further reduced at 473 K for 2h under a flow of hydrogen.

In order to determine the exact amount of Pd on our supports an X-ray fluorescence (XRF) analysis was carried out. Table 1 reports the metal loading found on the catalysts used.

Table 1 about here

2.2 Catalysts Characterization.

XRD data were acquired at room temperature on a Philips X-Pert diffractometer by using the Ni β-filtered CuKα radiation (λ=0.15418 nm). Analyses were performed on samples reduced at 473 K for 2h and registered in the 2θ range of 10–80° at a scan speed of 0.5°min^{-1}. Diffraction peaks were compared with those of standard compounds reported in the JPCDS Data File.

The particle size and the relative morphology of investigated catalysts were analysed by performing Transmission Electron Miscroscopy (TEM) measurements using a JEM-2100F (JEOL, Japan) operating at an acceleration voltage of 200 kV and directly interfaced with a computer controlled-CCD for real-time image processing. The specimens were prepared by grinding the reduced catalyst powder in an agate mortar and then suspending it in isopropanol. A drop of the suspension, previously dispersed in an ultrasonic bath for 1 hour, was deposited on a copper grid coated by a holey carbon film. After evaporation of the solvent, the specimens were introduced into the microscope column. Particle size distributions were obtained by counting several hundred particles visible on the micrographs on each sample. From the size distribution, the average diameter was calculated by using the expression: $d_n = \Sigma n_i d_i / n_i$ where n_i is the number of particles of diameter d_i.

H_2-TPR measurements were performed using a conventional TPR apparatus. The dried samples (50mg) were heated at a linear rate of 10 K min^{-1} from 298 to 1273 K in a 5vol % of H_2/Ar mixture at a flow rate of 20 cm^3 min^{-1}. H_2 consumption was monitored with a thermal conductivity detector (TCD). A molecular sieve cold trap (maintained at 193 K) and a tube filled with KOH, placed before the TCD, were used to block water and CO_2, respectively. The calibration of signals was done by injecting a known amount of H_2 into the carrier.

XPS measurements were performed on a JPS-9010MC photoelectron spectrometer using an Al Kα (1486.6 eV) radiation source. XPS spectra of reduced catalyst samples as well as those after in situ treatments at 100 Pa H_2 and 473 K for 4 h were recorded in an auxiliary reaction chamber.

After treatment, samples were introduced into the XPS chamber, avoiding exposure to air. In order to obtain the XPS spectra, pressure in the analysis chamber was maintained at $5x10^{-9}$ mbar. All spectra

were recorded at room temperature, and the binding energies (BE) were set taking the C 1s peak at 284.6 eV as reference. Peak deconvolution and fitting were performed using the peak-fitting software "SPECSURF, JEOL" including the spin-orbit splitting and relative intensities of the spin-orbit components fixed.

2.3 Catalytic Tests.

Hydrogenolysis reactions were performed in a 250 mL stainless steel autoclave at a stirring speed of 500 rpm. The reactor was purged with N_2 (99.99%), the system was then pressurized with the desired gas and, finally, heated up to the reaction temperature. The temperature was monitored using a thermocouple inserted into the autoclave and connected to the thermocontroller. The standard reaction was carried out under the following conditions: 453 K, 0.5 MPa initial N_2 pressure, 75 mL 4 wt % glycerol in isopropanol solution, and 500 mg catalyst previously reduced under H_2. After 24 hours of reaction, the system was cooled and, when at room temperature, the pressure was released carefully and the liquid was analyzed.

Product analysis was performed with a gas chromatograph (HP model 5890) equipped with a wide bore capillarity column (CP-WAX 52CB, 50 m, inner diameter 0.53 mm) and a flame ionization detector. The conversion and selectivity of glycerol were calculated on the basis of the following equations:

$$glycerol\ conversion(\%) = \frac{moles\ of\ reacted\ glycerol}{moles\ of\ glycerolfeed} \cdot 100$$

$$glycerol\ selectivity\ (\%) = \frac{moles\ of\ defined\ product}{moles\ of\ reacted\ glycerol} \cdot 100$$

3. Results

3.1 XRD analysis

XRD spectra of all investigated catalysts - after the reduction with H_2 at 473 K – are reported in Fig. 1.

Fig. 1 about here

As expected, in impregnated catalysts the diffraction peaks belonging to the corresponding support structures as well as metallic Pd species (2θ = 40.01) can be easily detected [12].

XRD patterns of catalysts prepared by coprecipitation reveal diffraction patterns related to Co_3O_4 and Fe_3O_4 [12]. The X-ray powder diffraction (XRD) pattern of the reduced PdCo catalyst shows strong and sharp diffraction peaks at 2θ values of 31.35, 36.98, 44.93, 59.52, and 65.36° corresponding to (220), (311), (400), (511), and (440) main crystal planes indicative of pure cubic crystalline Co_3O_4. In addition, it is possible to notice the presence of small diffraction peaks that can be ascribed to the presence of pure cubic crystalline cobalt monoxide (diffraction peaks at 2θ values of 42.52, 61.54 and 77.52°) as well as hexagonal metallic cobalt (diffraction peak at 2θ values of 47,09). In addition to that, the presence of broad (111), (200), and (220) peaks, slightly shifted toward higher angles from those reported for pure Pd, are definitely indicative of an interaction of palladium particles with the cobalt support, due to the formation of a Pd-Co alloy [13].

On the other hand, the absence of the (111) diffraction line of metallic palladium in the PdFe sample is indicative of extremely small Pd-particles highly dispersed [14].

3.2 HR-TEM analysis

Catalysts were also characterized by using HR-TEM (Fig. 2), which allows us to calculate the average size (Table 1) and the relative size distribution (Fig. 2) of palladium particles on the basis of size measurements of, at least, 100 particles for each sample.

The morphology of the supports is clearly in accord with XRD results. In addition, the d-spacing of planes in the HR-TEM lattice image of samples are in good agreement with those reported for pure Co_3O_4, CoO, Fe_2O_3 and Fe_3O_4 supports.

It appears also that, for impregnated catalysts reduced at 473 K, a broad distribution of palladium particles sizes is obtained. Although most of particles diameters are in a range between 3 and 6 nm, a small quantity (less than 5%) of large particles is also observed.

Conversely, the PdCo catalyst shows the presence of faceted metal particles and is characterized by a broader size distribution, with a mean diameter of 10.7 nm, higher than that of other samples.

On the contrary, PdFe exhibits a predominance of very small metallic particles and a relatively narrow particles sizes distribution with diameter values ranging between 0.5 and 2.5 nm, with particles of 1.2 nm being the most commonly measured size. This result can be related, in agreement with XRD results, to the preparation technique that allows ultra-small metal clusters Pd atoms formation.

Fig. 2 about here

3.3 H_2-TPR profiles

Fig. 3 shows H_2-TPR profiles of all investigated catalysts.

Fig. 3 about here

In Pd/Co_3O_4, Pd/CoO and Pd/Fe_2O_3 impregnated catalysts two peaks can be detected: the first at about 400 K belonging to the $Pd^{2+} \rightarrow Pd^0$ reduction (close to that of palladium acetylacetonate used as precursor in the catalysts preparation), the latter at 645, 695 and 585 K, respectively, attaining to the support reduction (weakly shifted towards lower temperatures with respect to that assigned to pure oxides [17, 18]).

Three characteristic H_2 consumption peaks appear in the Pd/Fe_3O_4 sample. While the peak at 940 K can be easily related to the support reduction, the other two peaks at 373 and 433 K may be attributed to: (i) the reduction of differently dispersed PdO species or (ii) a two steps reduction of PdO (Eqs1 and 2) [19].

$$2PdO + H_2 \rightarrow Pd_2O + H_2O \quad (1)$$

$$Pd_2O + H_2 \rightarrow 2Pd + H_2O \quad (2)$$

Since XPS experiments do not reveal the presence of Pd_2O species, the explanation of different dispersed PdO species is more feasible.

Hence, the TPR analyses of impregnated catalysts clearly indicate that poor interaction occurs between palladium and the supports.

On the other hand, H_2-TPR profiles of coprecipitated catalysts are characterized by only one broad and intense peak that can be related to the simultaneous reduction of palladium with cobalt-oxide or iron-oxide supports.

The profile of PdCo shows a broad and intense peak centered at about 535 K. This peak can be related to the simultaneous reduction of both palladium and cobalt cations causing shifts upward relative to that of palladium as compared to palladium oxide (PdO can be easily reduced by H_2 at room temperature) and downward relative to that of cobalt oxides (739 K) thus suggesting that: the Pd^{2+} species is stabilized within the cobalt-oxide support and the strong interaction between them facilitates the simultaneous reduction of Pd cation species and cobalt-oxide. This phenomenon is well documented in the literature and is attributed to strong interaction between well dispersed Pd particles and the metal oxide support [20]. Also the PdFe H_2-TPR profile is characterized by an reaction area centered at about 360 K that includes, as confirmed by our H_2 consumption calculations, both $Pd^{2+} \rightarrow Pd^0$ and $Fe^{3+} \rightarrow Fe_3O_4$ reductions. The large shift of the reduction temperature relative to the reaction $Fe^{3+} \rightarrow Fe_3O_4$ from 694 K to 352 K is therefore ascribed to palladium particles that catalyze the reduction of Fe^{3+} to the Fe_3O_4 structure.

Thus, H_2-TPR measurements suggest that, in the H_2 reduction of the coprecipitated samples, intimate interactions of palladium cations with metal oxides supports are present.

3.4 XPS analysis

The surface of all investigated catalysts was characterized by X-ray photoelectron spectroscopy (XPS).

XPS characterization was carried out in three different conditions: (a) "unreduced", (b) "reduced" at 473 K in H_2 and (c) "in situ-reduced" at 473K in H_2. The XPS curve-fitting results are summarized in Tables 2 and 3.

3.4.1 XPS analysis of the metal oxide supports.

Fig. 4 about here

Table 2 about here

Table 3 about here

The XPS spectra of unreduced, reduced and in situ-reduced impregnated samples show typical peaks of the starting support structures. This result, in agreement with H_2-TPR analysis, shows that there is no modification of the support upon H_2 reduction.

As far as the PdCo sample is concerned, since both components of the high-resolution Co 2p spectrum ($2p_{1/2}$ and $2p_{3/2}$) contain the same chemical information we focused our attention on the higher-intensity Co $2p_{3/2}$ band, including the shake-up satellite of the cobalt ions. Unreduced and reduced PdCo catalyst (Fig. 4(a) and Table 2) shows a broad peak at 780 eV, which corresponds to coexistence of Co^{II} and Co^{III}. The satellite peak at about 5.0 eV higher binding energy (785.0 eV) confirms the existence of cobalt(II)-oxide. Interestingly, after the in situ-reduction at 473 K, the disappearance of the satellite

peak at 785.0 eV as well as a shift to lower B.E. up to 778.0 eV, corresponding to the B.E. of the metallic cobalt [21, 22], was observed. This point is very interesting since a recent study on the reduction of Co_3O_4 catalyst in H_2 atmosphere indicates that the reaction $Co_3O_4 \rightarrow CoO$ proceeds at approximately 473K while the formation of metallic Co occurs only at higher temperature (up to 700K) [23]. In our case, the catalyst reduction is carried out at 473K; therefore the addition of palladium facilitates the support reduction. The XPS analysis concerning the PdCo catalysts is only apparently at variance with XRD results. The difference can be easily explained considering that XPS analysis is carried out under in-situ conditions allowing the reveal of metallic cobalt. Conversely, taking into account that the catalyst surface can be easily oxidized after exposure to air, XRD analysis shows mainly oxidized states of the support.

In the case of PdFe samples (Fig. 4 and Table 3), it is worth noting that on both "reduced" and "in situ reduced" samples the absence of the satellite peak at about 718.8 eV suggests a Fe_3O_4 structure, whereas its presence on the unreduced catalyst indicates the Fe_2O_3 composition [21].

3.3.2 XPS analysis of palladium species

In order to get insight into the electronic properties of supported Pd systems, XPS analysis over the Pd 3d binding energy (BE) region was carried out. Pd $3d_{5/2}$ binding energy (eV) values of all investigated catalysts are reported in Fig. 5 and are summarized in Table 2 and Table 3.

In all unreduced catalysts the binding energy of Pd $3d_{5/2}$ is at about 336.5 eV and can be attributed to Pd^{2+} species. This implies that on unreduced samples the palladium on the surface is completely oxidized to a PdO species.

Upon H_2 thermal treatment, binding energy values are shifted to lower binding energies as expected for metallic palladium. This phenomenon is well known and is related to the reduction, at higher temperature and under hydrogen atmosphere, of oxidized Pd species into metallic Pd.

The binding energy of the Pd $3d_{5/2}$ core level registered for reduced impregnated samples are close to 334.9-335 .0 eV very similar to that reported for pure metallic palladium [21].

On the contrary, the binding energy of Pd $3d_{5/2}$ level, in reduced coprecipitated catalysts, shows increased values of about 0.5 eV compared to those of bulk palladium. Higher binding energy than that of metallic palladium suggests that an electron transfer from Pd to the support occurs, resulting in a partial positively charged metal species ($Pd^{\delta+}$).

Slightly higher BE values for the Pd $3d_{5/2}$ core level have been reported for bimetallic supported Pd catalysts [24] and assigned to alloy formation. Similar results on analogous co-precipitated catalytic systems were recently reported by Tsang and co-workers [8] and, in the case of the analogous coprecipitated palladium catalyst, they emphasized that the progressive shift to higher binding energy values in the Pd $3d_{5/2}$ area can be related to the increasing amount of 'PdFe' clusters on the catalyst surface.

Fig. 5 about here

3.5 Catalytic tests

Analytical data referring to glycerol hydrogenolysis promoted by coprecipitated and impregnated catalysts, in absence of added hydrogen, are listed in Table 4. The hydrogen necessary for the hydrogenolysis reaction derives from the dehydrogenation of the solvent (2-propanol), induced by supported palladium catalysts as sketched in Fig. 6. In all experiments acetone was detected. However, in order to confirm the solvent oxidation, analogous catalytic tests (500 mg of catalysts, 453 K for 24 h) were carried out on pure 2-propanol under inert atmosphere: only acetone, besides very small quantities of other products, was formed and its amount changes in the order PdCo ≅ PdFe > $PdFe_2O_3$ ≅ Pd/Co_3O_4 > PdCoO.

Table 4 about here

Fig. 6 about here

The best conversion was achieved with coprecipitated samples that are more active in glycerol C-O bond breaking but less efficient in C-C bond cleavage (small amounts of EG are formed). When using PdCo and PdFe conversion of glycerol to 1-propanol is also observed indicating that the higher activity of substrates affords further hydrogenolysis of 1,2-PDO to 1-PO.

Finally, it is worth to underline that commercial Pd/SiO_2 and PdCoO show negligible activity with 1-hydroxyacetone as the only reaction product while the other investigated samples ($PdFe_3O_4$, $PdFe_2O_3$ and $PdCo_3O_4$) are generally much less active than coprecipitated catalysts with a selectivity distribution following the order AC ≥ 1,2-PDO > EG. Therefore, catalytic tests clearly indicate that coprecipitaed PdCo and PdFe catalysts are by far more efficient and selective towards 1,2-PDO than analogous impregnated samples.

4. Discussion

4.1 Correlation of catalyst structural properties with catalytic performance.

Factors effecting the catalytic performance are usually discussed in terms of: (i) overall surface area, (ii) metal particle size, (iii) dispersion of active metals, (iv) oxidation state of the metal centre, (v) nature of the support (unreducible/reducible, acid/base sites) and (vi) metal-metal and/or metal-support interactions. An accurate insight of all these parameters allows to discriminate which one is the most important factor in glycerol transfer hydrogenolysis.

Cross-check experiments show that pure Co_3O_4, CoO, Fe_3O_4 and Fe_2O_3 do not give noticeable glycerol conversion in absence of palladium particles under the identical conditions used in this study, suggesting that metal sites are an essential prerequisite for glycerol hydrogenolysis.

At the same time, the higher catalytic performances of coprecipitated catalysts with respect to analogous impregnated samples cannot be explained by the different surface area or particle size dimension observed, since Pd/SiO_2, with a specific surface area of 500 m^2/g was found to be nearly unactive towards glycerol hydrogenolysis.

Furthermore, coprecipitated samples show different metal particle size and uncomparable size distribution of Pd to consider these properties fundamental to interpret their catalytic activity. Rather, we need to look at the interaction between the metal and the support structure in order to find the right way for understanding the large gap in the observed reactivity. To this regard, we recall that XRD and XPS analyses clearly show that the metal-oxide support is easily reducible in coprecipitated PdFe and PdCo catalysts. In the case of the PdCo sample, when activated at 473 K with H_2, the support is reduced into the more stable Co_3O_4 structure.

Analogously the Fe_2O_3 support in PdFe catalyst, upon reduction, transforms into Fe_3O_4. In both cases, the reduction process is catalyzed by palladium particles as demonstrated by H_2-TPR experiments.

However, the most evident feature that allows to differentiate properties of coprecipitated catalysts from those of impregnated samples stays on the higher BE value of $Pd3d_{5/2}$ core level (Tables 2 and 3) observed for PdCo and PdFe substrates. These results, coupled with XPS detection of metallic cobalt in the PdCo sample, indicate possible formation of Pd-Co and Pd-Fe clusters that ensues electron modification on palladium particles making easier glycerol conversion.

Furthermore, cobalt based catalysts obtained from double layered Co-Zn-Al hydroxide, were found to be highly active and stable towards the hydrogenolysis of glycerol in aqueous media [25] and the role of iron as co-metal, in glycerol hydrogenolysis was recently reported to explain the high performance of the RuFe/CNT catalyst [26].

Even considering the complexity of coprecipitated catalysts structures, the preferential model deriving from on experimental results should be based on palladium nanoparticles tightly interacting with the support. The co-precipitation technique, used for the preparation of PdCo and PdFe catalysts, may

influence, in our opinion, the deposition of palladium ions or PdO nanoparticles embedded inside the support structure hence increasing the interactions between Pd and cobal/iron oxides and facilitating the formation of Pd-Co and Pd-Fe alloys by reduction.

The additional interesting point of the coprecipitated samples stems from the close correlation between glycerol conversion and acetone production from 2-propanol. Thus, the good performance of coprecipitated catalysts has to be attributed to two main factors: (i) the high ability to dehydrogenate 2-propanol into acetone and (ii) the high capability in C-O bond breaking.

As evidenced by H_2-TPR and XPS analysis, coprecipitated samples are characterized by palladium particles with different electronic properties than that of pure Pd. This electronic perturbation is a consequence of the electron transfer from Pd to Co and Fe which leads to a better interaction of palladium (positively charged) with the glycerol (where the -OH group is negatively polarized), weakening the C–O bond thus favoring the formation of hydroxyacetone. The presence of positively charged palladium is a crucial step in the overall reaction and it is consequence of bimetallic interaction.

In summary it should be definitely settled that, in transfer hydrogenolysis, the key factor raising the activity of coprecipitated catalysts is the strong interaction of palladium with the support leading to the formation of bimetallic ensembles. Other factors such as surface area, metal particle size, nature of the support, are definitely less important.

4.2 Transfer hydrogenolysis mechanism of glycerol by using 2-propanol as hydrogen source

Although several mechanisms have been suggested for glycerol hydrogenolysis, only few contributions are present in literature for CTH reactions [3b, 3c, 6a].

The proposed reaction mechanism (Scheme 1) has to take into account: (i) the formation of Pd-Co and Pd-Fe ensambles, (ii) the presence, in every experiments, of 1-hydroxy acetone, (iii) the dehydrogenation of 2-propanol and (iv) that the hydrogen concentration in the CTH reaction is relatively low compared with that occurring in presence of a high H_2 pressure.

The first step is glycerol chemisorption on the catalyst surface. Among the several possible conformers (the case of glycerol is very complex since 3 oxygen atoms with internal hydrogen bonds are present) computational studies [28-31] have established that the most preferred is the one having two adjacent OH groups bound to metal sites. In our case, it may occur through a strong adsorption of glycerol on Fe(Co) adjacent to Pd with two adjacent alcoholic groups of glycerol. The ensuing C-OH breaking, promoted by alloyed palladium, is then followed by internal rearrangement of the unstable enol intermediate (propene-1,2 diol) leading to AC. Generally speaking, the substitution of hydroxylic group by hydrogen in organic alcohols occurs through SN_1 and SN_2 mechanism, as reported for the hydrogenolysis of benzyl alcohol derivatives promoted by palladium systems [32]. In our case, the SN_2 path is to be considered quite unlikely since the hydrogen concentration (Pd-H sites) is relatively low under CTH conditions. As a consequence, only the SN_1 term (C-OH breaking) is operating. This is a quite rational route especially if we consider that the bond breaking energy of the primary C-OH group in the starting glycerol (79.6 kcal/mol) is strictly comparable with that of benzyl alcohol (~ 80 kcal/mol) and relatively much lower than that calculated for the analogous ethanol (93.5 kcal/mol) and the OH interaction with the catalyst surface is able to facilitate the C-OH bond breaking [33].

The involvement of AC in transfer hydrogenolysis reactions has raised numerous queries about its role in the overall mechanism. It was shown [3c] that a competitive adsorption between glycerol and hydroxyacetone can occur, preventing hydroxyacetone to undergo hydrogenation reaction to 1,2-PDO. Since in all our experiments hydroxyacetone was observed, it was important for us to confirm that AC can be converted into 1,2-PDO by supported palladium catalysts by using 2-PO as hydrogen donor. Once AC was allowed to react in 2-propanol under analogous reaction conditions in presence of PdCo and PdFe catalysts, (AC) was totally converted to 1,2-PDO confirming that AC is an intermediate in the conversion of glycerol into 1,2-PDO promoted by coprecipitated palladium catalysts in CTH conditions. The AC intermediate was adsorbed stably on the Fe (Co) sites to help the further reduction to 1,2-PDO.

The proposed mechanism involves, as final step, the transfer hydrogenation of AC to 1,2-PDO. This may occur through the direct transfer of hydrogen from 2-propanol to AC mediated by the catalytic surface (Scheme 1 c-1) or by the transfer of hydrogen atom from Pd-H species (formed by dehydrogenation of 2-propanol) to the carbonyl double bond, as it normally occurs in classical hydrogenation reactions (Scheme 1 c-2).

The first route is generally accounted in homogeneous phase [34] and was recently thoroughly demonstrated to occur also under heterogeneous conditions [35] in the transfer hydrogenation of cellulose-based oligomers.

Scheme 1 about here

5. Conclusions

The catalytic transfer hydrogenolysis (CTH), promoted by supported palladium catalysis was investigated. Coprecipitated palladium catalysts on cobalt oxide and iron oxide supports allow a complete conversion of glycerol to 1,2-propanediol and ethylene glycol under mild reaction conditions by using 2-propanol as hydrogen donor. Analogous impregnated samples as well as commercial Pd/SiO_2 catalyst were found to be poor active in CTH reactions. A tight correspondence between the tendency of catalysts to dehydrogenate 2-propanol and the ability to afford CTH reactions was also found.

The physico-chemical characterization of the broad set of Pd catalysts chosen allows us to conclude that the coprecipitation method allows a strong interaction between palladium and support leading to formation of bimetallic ensambles that positively promote the glycerol CTH reaction.

The catalytic tests clearly evidence that hydroxyacetone is an intermediate in the CTH of glycerol so that it is possible to conclude that the most convincing mechanism involves the C-OH breaking of the primary alcoholic group promoted by surface palladium atoms leading to hydroxyacetone that is then reduced to 1,2-propanediol.

Acknowledgements

The financial support by Catalysis Research Center, Hokkaido University (Overseas Research Fellow 2013) and MIUR (PRIN2010) are gratefully acknowledged. The authors express thanks to the technical support of the CRC Technical division for the XPS and TEM measurements.

References

(1) (1a) C. O. Tuck, E. Pérez, I. T. Horváth, R. A. Sheldon, M. Poliakoff Science, 2012, 337, 695-699; (1b) P.Gallezot Chem. Soc. Rev., 2012, 41, 1538-1558

(2) (2a) Agnieszka M. Ruppert, Kamil Weinberg, and Regina Palkovits, Angew. Chem. Int. Ed. 2012, 51, 2564 – 2601; (2b) N. Yan and P. J. Dyson, Current Opinion in Chemical Engineering 2013, 2:178–183; (2c) J. Ten Dam, U Hanefeld ChemSusChem 2011, 4, 1017-1034; (2d) J.P. Ma, W.Q. Yu, M. Wang, X.Q. Jia, F. Lu, J. Xu Chinese Journal of Catalysis 2013, 34, 492-507

(3) (3a) Jae, W. Zheng, R. F. Lobo and D. G. Vlachos, ChemSusChem 2013, 6, 1158 – 1162;, (3b) A. Martin, U. Armbruster, Inaki Gandarias, P. L. Arias Eur. J. Lipid Sci. Technol. 2013, 115, 9–27; (3c) Gandarias, P.L. Arias, J. Requies, M. El Doukkali, M.B. Güemez Journal of Catalysis 282 (2011) 237–247.

(4) (4a) M. Pagliaro, M. Rossi, The Future of Glycerol (2nd Edition), Royal Society of Chemistry, Cambridge, 2010; (4b) Z. Y. Zakaria, N. A. S. Amina, J. Linnekoski Biomass and Bioenergy 55 (2013) 370-385; (5c) N.H. Tran and G.S.K. Kannangara, G.S.K. Chem. Soc. Rev. (2013) 42, 9454-9479; (4d) C.H. Zhou, H. Zhao, D. S. Tong, L. M. Wu, W. H. Yu, Catalysis Reviews: Science and Engineering, 2013, 55

(5) (5a) C.-H Zhou, J. N. Beltramini, Y.-X. Fan, G. Q. Lu, Chem. Soc. Rev. 2008, 37, 527 – 549; (5b) Y. Nakagawa, K. Tomishige, Catalysis Science and Technology (2011), 1, 179-190; F. Mauriello, (5c) M. G. Musolino, R. Pietropaolo in Glycerol: Production, Structure and Applications (Miguel De Santos Silva and Paulo Costa Ferreira) Nova Publisher (2012), 45-76.

(6) J. Liu, B. Sun, J. Hu, Y. Pei, H. Li, M. Qiao, Journal of Catalysis 2010, 274, 287–295;

(7) C-T Wu, K. M. K. Yu, F. Liao, N. Young, P. Nellist, A. Dent, A. Kroner, S. C. E. Tsang Nature Commun. 2012, 3, 1050

(8) M.G. Musolino, C. Busacca, F. Mauriello, R. Pietropaolo Applied Catalysis A: General 2010, 379, 77-86.

(9) (9a) Scholz, D., Aellig, C. and Hermans, I. (2013) Catalytic Transfer Hydrogenation/Hydrogenolysis for Reductive Upgrading of Furfural and 5-(Hydroxymethyl)furfural. ChemSusChem. doi: 10.1002/cssc.201300774; (9b) J. Ge, Z. Zeng, F. Liao, W. Zheng, X. Hong and S. C. E. Tsang Green Chem., 2013, 15, 2064–2069

(10) (10a) M. G. Musolino, L. A. Scarpino, F. Mauriello and R. Pietropaolo, Green Chem., 2009, 11, 1511-1513; (10b) M. G. Musolino, L. A. Scarpino, F. Mauriello, R. Pietropaolo, ChemSusChem, 4, 1143-1150, 2011.

(11) F. Schüth, M. Hesse, K. K. Unger, Handbook of Heterogeneous Catalysis, 2008 Wiley-VCH Verlag GmbH & Co. KGaA.

(12) International Center for Diffraction Data, Powder Diffraction Database, Pennsylvania, PA, 1997

(13) M. Vondrova, T. Klimczuk, V. L. Miller, B. W. Kirby, N. Yao, R. J. Cava, A.B. Bocarsly Chem. Mater. 2005, 17, 6216-6218

(14) L.S.F. Feio, C.E. Hori, L.V. Mattos, D. Zanchet, F.B. Noronha, J.M.C. Bueno, Applied Catalysis A: General 348, 2008, 183–192

(15) G. Kyriakou, M. B. Boucher, A. D. Jewell, E. A. Lewis, T. J. Lawton, A. E. Baber, H. L. Tierney, M. Flytzani-Stephanopoulos, E. C. H. Sykes *SCIENCE 2012, 335, 1209-12012*

(16) B. Qiao, A. Wang, X. Yang, L. F. Allard, Z. Jiang, Y. Cui, J. Liu, J. Li and T. Zhang NATURE CHEMISTRY | VOL 3 | AUGUST 2011, 634-641.

(17) Zhang B C, Tang X L, Li Y, Cai W J, Xu Y D, Shen W J. Catal Commun, 2006, 7(6): 367

(18) (20a) Zielinski, J.; Zglinicka, I.; Znak, L.; Kaszkur, Z. Appl. Catal., A: Gen. 2010, 381 (1−2), 191− 196. (20b) Lin, H.-Y.; Chen, Y.-W.; Li, C. Thermochim. Acta 2003, 400 (1−2), 61−67

(19) C.-Wei Chou, Shou-Juan Chu, Hui-Jean Chiang, Chien-Yu Huang, Chiu-jung Lee, Shyang-Roeng Sheen, Tsong P. Perng, and Chuin-tih Yeh, J Phys Chem C 105, 2001, 9113

(20) F.B. Noronha, M. Schmal, C. Nicot, B. Moraweck, R. Fréty Journal of Catalysis, 168, 1997, 42–50.

(21) Handbook of X-ray Photoelectron Spectroscopy C. D. Wanger, W. M. Riggs, L. E. Davis, J. F. Moulder and G. E.Muilenberg Perkin-Elmer Corp., Physical Electronics Division, Eden Prairie, Minnesota, USA, 1979.

(22) B. Ernst, A. Bensaddik, L. Hilaire, P. Chaumette, A. Kiennemann Catalysis Today 39 (1998) 329-341; Jae-Chun Ryu, Dong-Hee Lee, Kyoung-Soo Kang, Chu-Sik Park, Jong-Won Kim, Young-Ho Kim J. of Ind. And Eng. Chemistry 14 (2008) 252.

(23) M. R. Ward, E. D. Boyes and Pratibha L. Gai, ChemCatChem 2013, 5, 2655–2661

(24) (24a) M. L. Cubeiro and J. L. G. Fierro JOURNAL OF CATALYSIS 179, 150–162 (1998); (24b) K. Sun, W. Lu, M. Wang, X. Xu, Appl. Catal. A 2004, 268, 107 – 113; (24c) A. F. Carlsson, M. Naschitzki, M. Ba1umer, and H.-J. Freund J. Phys. Chem. B 2003, 107, 778-785; (24d) M. S. Yalfani, S. Contreras, J. Llorca, M. Dominguez, J. E. Sueirasa and Francesc Medina Phys. Chem. Chem. Phys., 2010, 12, 14673–14676; (24e) S. Marx and A. Baiker J. Phys. Chem. C 2009, 113, 6191–6201

(25) X. Guo, Y. Li, W. Song, W. Shen Catal Lett (2011) 141:1458–1463

(26) B. Li, J. Wang, Y. Yuan, H. Ariga, S. Takakusagi, and K. Asakura ACS Catal. 2011, 1, 1521–1528

(27) J. A. Schwarz, C. Contescu, A. Contescu, Chem Rev. 95 (1995), 477-510

(28) J. Auneau, C. Michel, F. Delbecq, C. Pinel and P. Sautet Chem Eur Journal, 2011, 17, 14288 – 14299

(29) D. Coll, F. Delbecq, Y. Arayb and P. Sautet Phys. Chem. Chem. Phys., 2011, 13, 1448–1456;

(30) B. Liu, J. Greeley Phys. Chem. Chem. Phys., 2013, 15, 6475—6485

(31) C. Hadad, C. Callam, S. Singer and T. Lowary, J. Am. Chem. Soc., 2001, 123, 11743

(32) (32a) N. Thakar, N. F. Polder, K. Djanashvili, H. van Bekkum, F. Kapteijn, J. A. Moulijn, J. Catal. 2007, 246, 344-350; (32b) M.G. Musolino, F. Mauriello, C. Busacca, R. Pietropaolo, unpublished results.

(33) Comprehensive Handbook of Chemical Bond Energies. Yu-Ran Luo. CRC Press 2007.

(34) S. M. Samec, J.-E. Backvall, P. G. Andersson, P. Brandt, Chem. Soc. Rev. 2006, 35, 237 – 248.

(35) A.Shrotri, H. Kobayashi, A. Tanksale, A. Fukuoka, J. Beltramini ChemCatChem 2014, 6, 1349 – 1356

Table 1

Main characteristics of the supported palladium catalysts investigated (S.A. = surface area; d_n = Mean particle size from TEM).

Catalyst notation	**Support**	**Catalyst source/preparation**	**Pd loading (wt%)**	**S.A. (m^2/g)**	**d_n (nm)**
PdCo	Co_3O_4	co-precipitation	3.7	106	10.7
Pd/CoO	CoO	impregnation	4.5	8	4.3
Pd/Co_3O_4	Co_3O_4	impregnation	5.1	70	7.8
PdFe	Fe_3O_4	co-precipitation	8.7	170	1.8
Pd/Fe_3O_4	Fe_3O_4	impregnation	5.2	60	8.8
Pd/Fe_2O_3	Fe_2O_3	impregnation	5.5	6	7.1
Pd/SiO_2	SiO_2	commercial	5	400	12.2

Table 2

Binding energy values of Pd 3d5/2, Co2p3/2 and O1s in PdCo, PdCoO and $PdCo_3O_4$ catalysts.

Catalysts notation		**Binding Energy (eV)**			
		$Pd3d_{5/2}$	**$Co2p_{3/2}$**	**$Co2p_{3/2}$ sat.**	**O1s**
PdCo	*unred*	336.8	779.9	-	531.4
	red	335.2	779.7		530.4
	in situ red	335.5	778.2	785.9	530.4
PdCoO	*unred*	337.1	780.1	786.0	531.4
	red	334.9	780.1	786.0	531.4
	in situ red	334.9	780.1	786.0	531.4
$PdCo_3O_4$	*unred*	337.2	780.1	786.1	531.4
	red	335.0	780.1	786.1	531.4
	in situ red	335.0	780.1	786.1	531.4

Table 3

Binding energy values of Pd 3d5/2, Fe2p3/2, O1s and C1s in PdFe, $PdFe_3O_4$ and $PdFe_2O_3$ catalysts.

Catalysts notation		**Binding Energy (eV)**			
		$Pd3d_{5/2}$	**Fe2p3/2**	**Fe2p3/2 sat.**	**O1s**
PdFe	*unred*	336.5	710.9	718.5	530.2
	red	335.2	710.7	-	530.2
	in situ red	335.3	710.7	-	530.2
$PdFe_3O_4$	*unred*	336.5	710.5	-	530.1
	red	334.8	710.5	-	530.1
	in situ red	334.8	710.5	-	530.0
$PdFe_2O_3$	*unred*	336.6	710.4	718.4	530.0
	red	334.8	710.4	718.5	530.0
	in situ red	334.8	710.4	718.5	530.0

Table 4

Glycerol transfer hydrogenolysis promoted by supported palladium catalysts, carried out at 453 K and 0.5 MPa N_2 pressure for 24 h. 1,2-PDO = 1,2-propanediol; EG = ethylene glycol; 1-PO = 1-propanol; AC = 1-hydroxyacetone; OP = other products

Catalysts notation	**Conversion (%)**	**Selectivity (%)**				
		1,2-PDO	**EG**	**1-PO**	**AC**	**OP**
PdCo	100	63.98	8.19	24.91	-	2.91
$PdCo_3O_4$	37,9	14.6	6.1	1.2	37.4	40.8
PdCoO	2.9	-	-	-	100	-
PdFe	100	55.93	5.77	10.11	25.19	3.0
$PdFe_3O_4$	66.5	47.7	8.0	0	44.3	0
$PdFe_2O_3$	40.4	26,6	6.6	-	58.1	8.7
$PdSiO_2$	0.5	-	-	-	100	-

Figure captions

Fig. 1. XRD patterns of the investigated palladium catalysts.

Fig. 2. TEM images of coprecipitated and impregnated palladium catalysts.

Fig. 3. H_2-TPR profiles of the investigated palladium catalysts.

Fig. 4. The XPS Co $2p_{3/2}$ and Fe $2p_{3/2}$ in PdCo and PdFe catalysts: unreduced (a), reduced (b) and in situ reduced (c).

Fig. 5. The XPS Pd$2p_{3/2}$ of coprecipitated and impregnated catalysts.

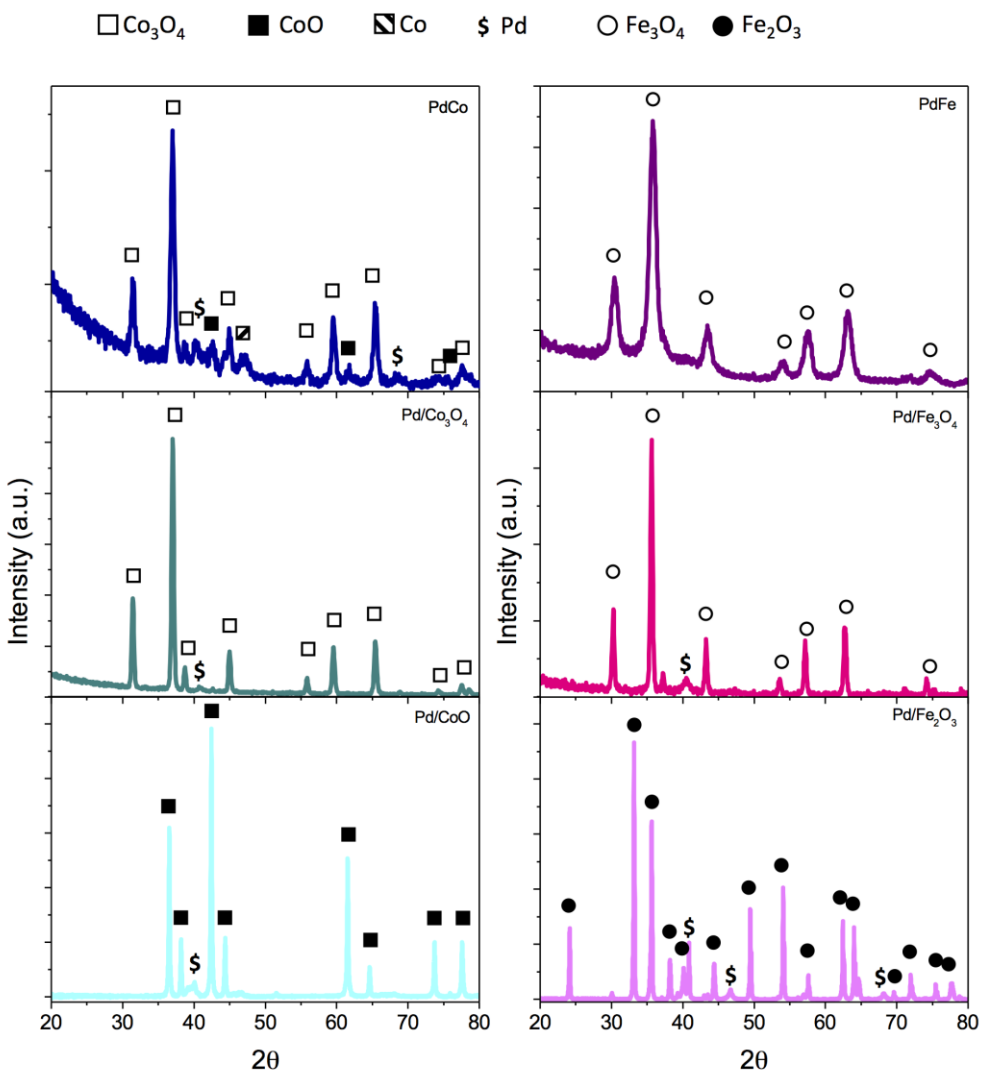

Fig. 1. XRD patterns of the investigated palladium catalysts.

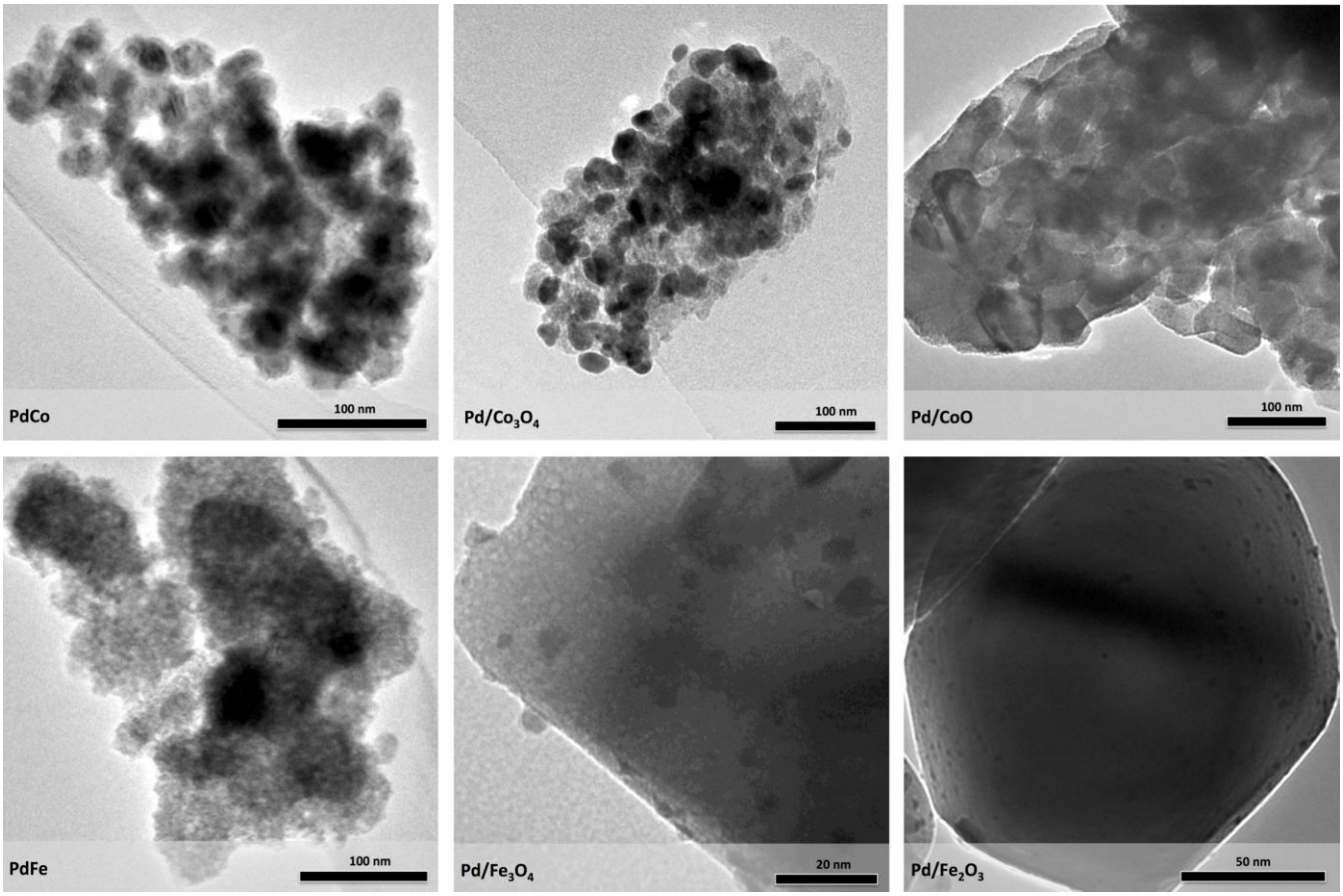

Fig. 2. TEM images of coprecipitated and impregnated palladium catalysts.

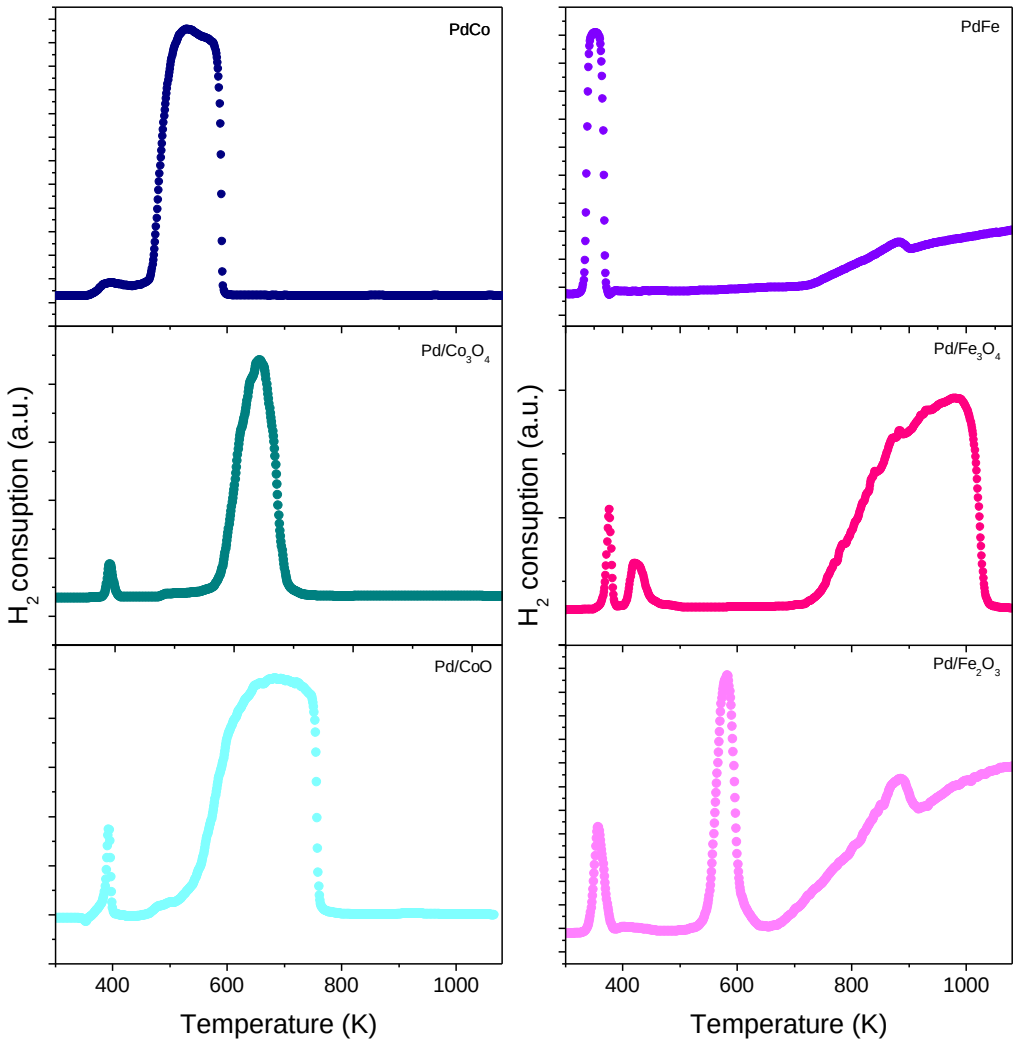

Fig. 3. H_2-TPR profiles of the investigated palladium catalysts.

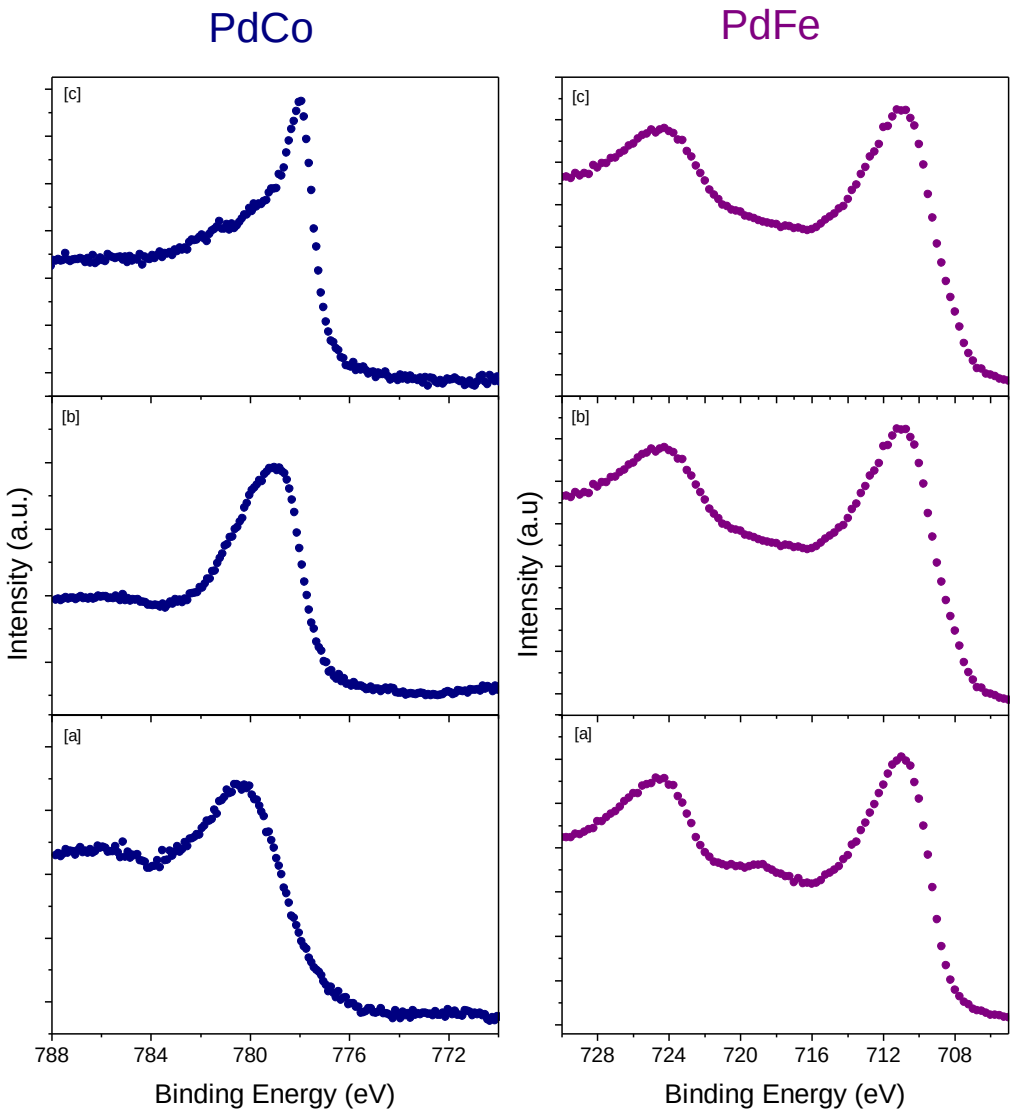

Fig. 4. The XPS Co $2p_{3/2}$ and Fe $2p_{3/2}$ in PdCo and PdFe catalysts: unreduced (a), reduced (b) and in situ reduced (c).

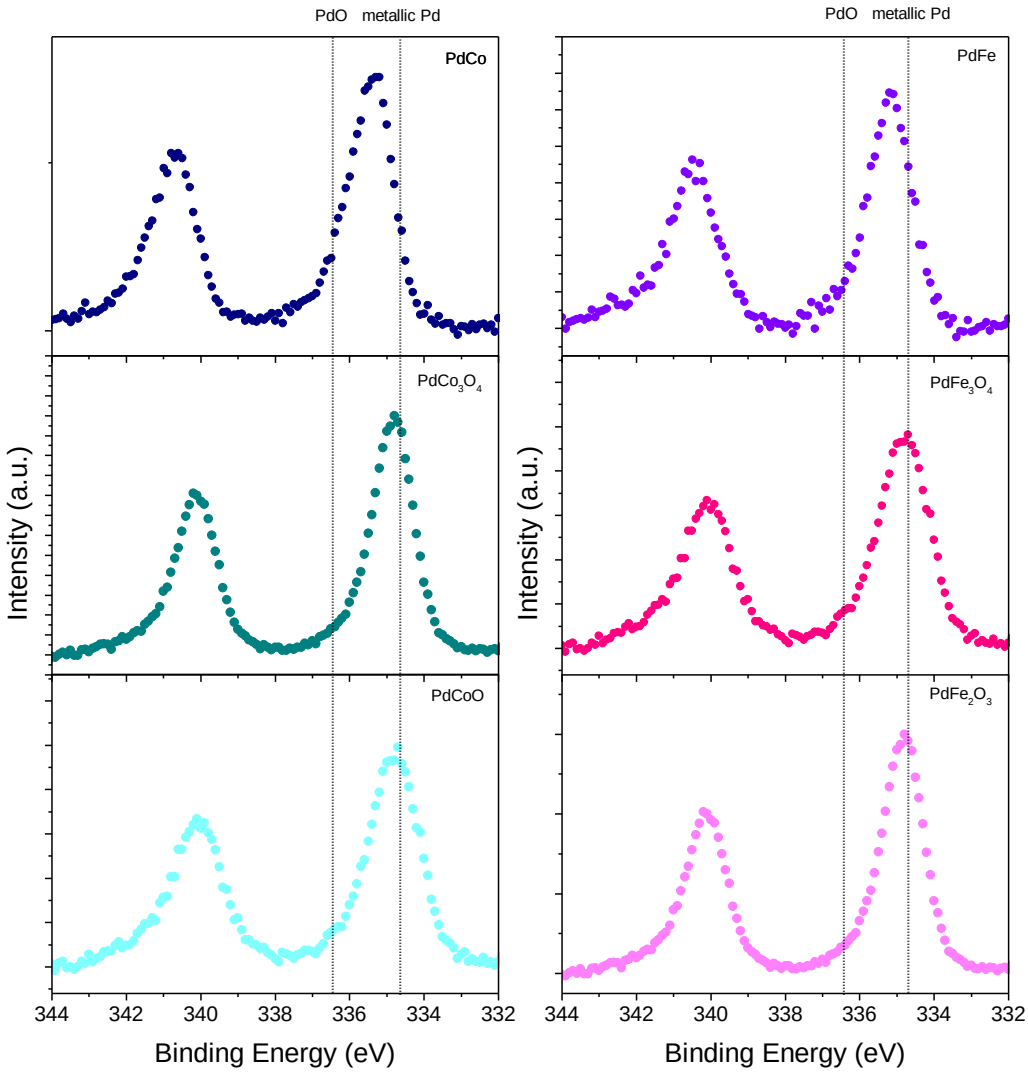

Fig. 5. The XPS Pd2p$_{3/2}$ of coprecipitated and impregnated catalysts.

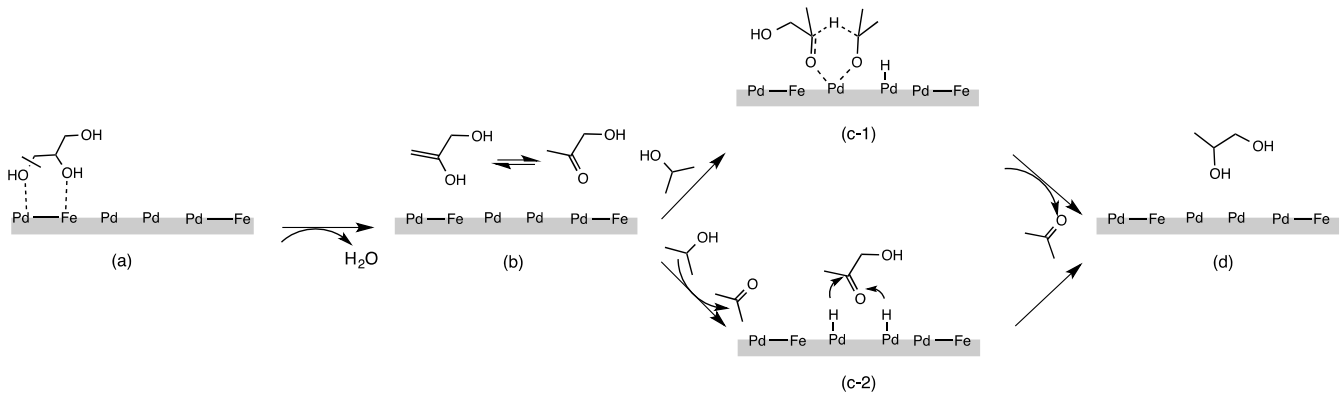

Scheme 1